MELTING HEAT TRANSFER IN A VERTICAL RECTANGULAR ENCLOSURE WITH A CONDUCTIVE WALL

R.Y. Sakr
Mechanical Engineering Department
Shoubra Faculty of Engineering, Zagazig University, Cairo, Egypt

Abstract:

A numerical study has been developed to analyze the wall conduction effect on natural convection heat transfer in a two dimensional vertical enclosure filled with phase change material (PCM) undergoing a melting process. One vertical wall of the enclosure is kept isothermally at a temperature higher than that of the phase change temperature while the other walls are kept insulated. A mathematical model has been developed based on the coupling of the equations that govern the phenomenon. The finite element method is used to develop this model to solve the transient behavior of melting phenomenon. Body-fitted curvilinear coordinates are used for treating the moving boundary (melting front). The effects of void fraction, i.e. wall thickness, wall and PCM thermophysical properties and Rayleigh number on the heat transfer characteristics and melting rate are investigated.

Results obtained from this model have been verified through a comparison with those available in the existing publications. A new correlation equation for the average Nusselt number based on the total heat input with the melting rate, void fraction, wall and PCM thermophysical properties and operating conditions is derived. Other different correlation equations for the average Nusselt number at the wall-liquid phase interface and the melting rate based on the numerical results are also presented.

Keywords: Wall Conduction – Melting – Natural Convection – Modelling

1. INTRODUCTION

Conjugate heat transfer problems involving solid-liquid phase change in enclosures with natural convection in liquid phase has recently received considerable research attention. This is due to large number of applications, including latent heat storage, material processing, crystal growth, castings of metals, glass industry, purification of materials, and others. The prediction of temperature distribution and melting-solidification rate is very important in some modern technologies. This is in order to control the fundamental parameters such as the speed of fabrication, incidence of defects as well as the influence on the final properties of products and the possibility of damage of the contact surface between the wall and phase change material.

An increasing number of experimental and numerical studies have been performed on the coupled problem of phase change with natural convection in the melt layer and without wall conduction effect [1-4]. In these studies, the solid phase is maintained at the fusion temperature and the influence of heat conduction in the solid phase change material is not considered. The combined effects of natural convection in the liquid and the heat conduction in the solid phase of PCM have been studied for melting of ordinary

non-metallic solid [5,6], and melting of metallic solid [7]. The effect of liquid superheating during solidification in a square cavity is studied numerically by Rady et al.[8].

The effect of wall conduction on natural convection heat transfer without phase change in enclosures is studied experimentally by Olson and Glicksman [9], and numerically by [10, 11, 12]. A perturbation solution for the phase change problem during solidification involving the wall conduction and wall-PCM interfacial thermal contact resistance is introduced by Hawang et al. [13]. But their study was limited to the classical Stefan problem, i.e. neglecting natural convection in the liquid phase. Many important physical heat transfer processes that occur across the liquid-solid interface during phase change have not been adequately studied and are not well understood. From the above, it can be concluded that, there is a shortage in the literature concerning with the effect of wall conduction on the melting heat transfer characteristics that consider the natural convection in the liquid phase.

The purpose of the present paper is to examine numerically the influence of wall conduction material (non-metallic and metallic) on the rate of heat transfer and the rate of melting of the phase change material. Vertical cavity configuration was chosen because of fundamental interest and numerous applications. Also, the effect of Rayleigh number, Stefan number, wall to liquid phase thermal conductivity ratio, wall to liquid thermal diffusivity ratio, and void fraction on the average Nusselt number and the melting rate is investigated.

2. MATHEMATICAL FORMULATION

2.1 Physical Model and Assumptions

The proposed system is a rectangular enclosure preceded by an isothermal, vertical wall of definite thickness and having a finite thermal conductance. The other sides of the enclosure are kept adiabatically. A phase change material (PCM) is contained in the enclosure. The geometry of the physical system and coordinate system are shown in Fig. (1). The height of enclosure is denoted by H_2, the width by H_1 and the wall thickness by H_3. Dimension of the enclosure normal to the plane of the diagram is assumed to be long. Hence, the problem can be considered to be a two-dimensional problem. The location of melting front at time t, is represented by S=S (y, t). The following assumptions are made:

1-The thermophysical properties of the wall material and PCM are independent of temperature.
2- Boussinesq approximation is assumed to be valid in the liquid phase of PCM.
3- Volume change due to solid-liquid phase change is negligible.
4-Liquid is assumed to be Newtonian and incompressible.
5-Fluid motion in the melt is considered to be laminar.

2.2 Governing Equations and Coordinate Transformation

A-For the wall

$$\rho_w c_w \frac{\partial T_w}{\partial t} = k_w \left(\frac{\partial^2 T_w}{\partial x^2} + \frac{\partial^2 T_w}{\partial y^2} \right) \qquad (1)$$

B-For the liquid phase of PCM

The conservation of mass, momentum, and energy for the liquid phase can be written as follows:

(I) Mass conservation

$$\frac{\partial u}{\partial x}+\frac{\partial v}{\partial y}=0 \tag{2}$$

(II) Momentum conservation

a- X-Direction

$$\frac{\partial u}{\partial t}+u\frac{\partial u}{\partial x}+v\frac{\partial u}{\partial y}=-\frac{1}{\rho}\frac{\partial p}{\partial x}+\nu\left(\frac{\partial^2 u}{\partial x^2}+\frac{\partial^2 u}{\partial y^2}\right) \tag{3-a}$$

b- Y Direction

$$\frac{\partial v}{\partial t}+u\frac{\partial v}{\partial x}+v\frac{\partial v}{\partial y}=g\,\beta\,(T-T_o)-\frac{1}{\rho}\frac{\partial p}{\partial y}+\nu\left(\frac{\partial^2 v}{\partial x^2}+\frac{\partial^2 v}{\partial y^2}\right) \tag{3-b}$$

(III) Energy conservation

$$\rho_L c_L\left(\frac{\partial T_L}{\partial t}+u\frac{\partial T_L}{\partial x}+v\frac{\partial T_L}{\partial y}\right)=k_L\left(\frac{\partial^2 T_L}{\partial x^2}+\frac{\partial^2 T_L}{\partial y^2}\right) \tag{4}$$

C-For the solid phase of PCM

$$\rho_S c_S\frac{\partial T_S}{\partial t}=k_S\left(\frac{\partial^2 T_S}{\partial x^2}+\frac{\partial^2 T_S}{\partial y^2}\right) \tag{5}$$

By eliminating the pressure between the two momentum equations (3-a) and (3-b) and introducing the definitions for vorticity and stream function in the following equations:

$$\omega=\left(\frac{\partial v}{\partial x}-\frac{\partial u}{\partial y}\right) \tag{6}$$

$$u=\frac{\partial \psi}{\partial y}\ ,\quad v=-\frac{\partial \psi}{\partial x} \tag{7}$$

The main feature of the melting/solidification problems is the geometrical changes and movements of the irregular melting/solidification front interface. One resolution of this difficulty is to perform an immobilization transformation of coordinates. This simplifies the numerical analysis by transforming the irregular boundary to a fixed one of much simpler geometry, at the expense of complicating the governing equations. So, the problem of discretization at each time step is avoided. Introducing the general Oberkampf transformation [14] as follows:

$$\xi=\frac{x-x_l(y)}{x_u(y)-x_l(y)}\ ,\quad \eta=\frac{y-y_l(x)}{y_u(x)-y_l(x)} \tag{8}$$

And applying this transformation for both phases of PCM, the following equations are obtained:

$$\xi_1=\frac{x}{S(y,t)},\ \eta_1=\frac{y}{H_2} \tag{9}$$

for the first phase (liquid phase)

$$\xi_2 = \frac{x - S(y,t)}{H_1 - S(y,t)},\ \eta_2 = \frac{y}{H_2} \tag{10}$$

for the second phase (solid phase)
let for the wall

$$\xi_w = \frac{x}{H_2}, \eta_w = \frac{y}{H_2} \tag{11}$$

The following are the dimensionless variables and groups appearing in the phenomenon and selecting suitable reference values for length, velocity, stream function, and vorticity

$$X = \frac{S(y,t)}{H_2},\ U = \frac{u}{U_o},\ V = \frac{v}{U_o},\ \Theta = \frac{T - T_F}{T_H - T_F},\ Ste^* = \frac{c_L(T_{W-L} - T_F)}{L}, Ste = \frac{c_L(T_H - T_F)}{L}$$

$$U_o = \frac{\alpha_L}{H_2},\ Pr = \frac{\nu}{\alpha_L},\ \Psi = \frac{\psi}{\alpha_L},\ \Omega = \frac{\omega}{\alpha_L/H_2},\ Ra = \frac{g\beta(T_H - T_F)H_2^3}{\nu\,\alpha_L}, \tau = \frac{\alpha_L\, t}{H_2^2}$$

$$k^*_{S-L} = \frac{k_S}{k_L},\ \alpha^*_{S-L} = \frac{\alpha_S}{\alpha_L},\ k^*_{W-L} = \frac{k_W}{k_L},\ \alpha^*_{W-L} = \frac{\alpha_W}{\alpha_L},\ \rho^*_{S-L} = \frac{\rho_S}{\rho_L},\ Ra^* = \frac{g\beta(T_{W-L} - T_F)H_2^3}{\nu\alpha_L}$$

The immobilized normalized transformed equations for temperature, vorticity, and stream function are as follows:

A: Liquid phase of PCM

(i) Temperature Equation:-

$$\left(\frac{1}{X^2} + \frac{\xi^2 X'^2}{X^2}\right)\frac{\partial^2\Theta_L}{\partial\xi^2} - \frac{2\xi X'}{X}\frac{\partial^2\Theta_L}{\partial\xi\partial\eta} + \frac{\partial^2\Theta_L}{\partial\eta^2} + \left(\frac{2\,\xi X'^2}{X^2} - \frac{\xi X''}{X}\right)\frac{\partial\Theta_L}{\partial\xi} = \frac{\partial\Theta_L}{\partial\tau} - \frac{\xi\dot{X}}{X}\frac{\partial\Theta_L}{\partial\xi} +$$
$$\left(\frac{1}{X}\frac{\partial\Psi}{\partial\eta} - \frac{\xi X'}{X^2}\frac{\partial\Psi}{\partial\xi}\right)\frac{\partial\Theta_L}{\partial\xi} + \left(\frac{\xi X'}{X^2}\frac{\partial\Theta_L}{\partial\xi} - \frac{1}{X}\frac{\partial\Theta_L}{\partial\eta}\right)\frac{\partial\Psi}{\partial\xi} \tag{12}$$

(ii) Vorticity Equation:-

$$\frac{\partial\Omega}{\partial\tau} - \frac{\xi\dot{X}}{X}\frac{\partial\Omega}{\partial\xi} + \frac{1}{X}\left(\frac{-\xi X'}{X}\frac{\partial\Psi}{\partial\xi} + \frac{\partial\Psi}{\partial\eta}\right)\frac{\partial\Omega}{\partial\xi} - \frac{1}{X}\frac{\partial\Psi}{\partial\xi}\left(\frac{-\xi X'}{X}\frac{\partial\Psi}{\partial\xi} + \frac{\partial\Psi}{\partial\eta}\right) = Ra^*\,Pr\left(\frac{1}{X}\frac{\partial\Theta_L}{\partial\xi}\right)$$
$$+ Pr\left(\frac{1}{X^2}\frac{\partial^2\Omega}{\partial\xi^2} + \frac{\xi^2(X')^2}{X^2}\frac{\partial^2\Omega}{\partial\xi^2} - \frac{2\xi X'}{X}\frac{\partial^2\Omega}{\partial\xi\partial\eta} + \frac{\partial^2\Omega}{\partial\eta^2} + \left\{\frac{2\xi(X')^2}{X^2} - \frac{\xi X''}{X}\right\}\frac{\partial\Omega}{\partial\xi}\right) \tag{13}$$

(iii) Streamline Equation:-

$$\left(\frac{1}{X^2} + \frac{\xi^2(X')^2}{X^2}\right)\frac{\partial^2\Psi}{\partial\xi^2} - \frac{2\xi X'}{X}\frac{\partial^2\Psi}{\partial\xi\partial\eta} + \frac{\partial^2\Psi}{\partial\eta^2} + \left(\frac{2\xi(X')^2}{X^2} - \frac{\xi X''}{X}\right)\frac{\partial\Psi}{\partial\xi} = -\Omega \tag{14}$$

(B): Solid phase of PCM

$$\left(\frac{1}{(1/A_R - X)^2}+\frac{(\xi-1)^2(X')^2}{(1/A_R-X)^2}\right)\frac{\partial^2\Theta_S}{\partial\xi^2}+\frac{2(\xi-1)X'}{(1/A_R-X)}\frac{\partial^2\Theta_S}{\partial\xi\partial\eta}+\frac{\partial^2\Theta_S}{\partial\eta^2}+$$
$$\left(\frac{2(\xi-1)(X')^2}{(1/A_R-X)^2}+\frac{(\xi-1)X''}{(1/A_R-X)}\right)\frac{\partial\Theta_S}{\partial\xi}-\frac{(\xi-1)X}{(1/A_R-X)}\frac{\partial\Theta_S}{\partial\xi}=\frac{\partial\Theta_S}{\partial\tau} \quad (15)$$

Where;

$$X'=\frac{\partial X}{\partial\eta},\quad X''=\frac{\partial^2 X}{\partial\eta^2},\quad \dot{X}=\frac{\partial X}{\partial\tau},\ A_R=\frac{H_2}{H_1}$$

(C) Conductive wall

$$\frac{\partial\Theta_W}{\partial\tau}=\alpha^*_{W-L}\left(\frac{\partial^2\Theta_W}{\partial\xi^2}+\frac{\partial^2\Theta_W}{\partial\eta^2}\right) \quad (16)$$

2.3 Boundary Conditions

1- Temperature boundary conditions

$$\Theta=\Theta_W=1.0 \quad \text{on } \Gamma_1$$
$$\frac{\partial\Theta}{\partial\eta}=0.0 \quad \text{on } \Gamma_2 \text{ and } \Gamma_4$$
$$\frac{\partial\Theta}{\partial\xi}=0.0 \quad \text{on } \Gamma_3 \quad (17)$$

2- Stream function boundary conditions

On all liquid boundaries

$$\Psi_w = 0.0 \quad (18)$$

3- Vorticity boundary conditions

On all liquid boundaries

$$\Omega_w=\frac{2(\Psi_{w+1}-\Psi_w)}{(\Delta N)^2} \quad (19)$$

Where;

w refers to the nodal value at the no slip wall.

w+1 refers to the adjacent interior node.

ΔN is the dimensionless distance separating this node pair.

4- Boundary conditions for the moving interface

$$\Theta_L=\Theta_S=0.0 \quad (20\text{-a})$$

The heat balance at the solid-liquid interface gives:

$$\frac{\partial X}{\partial\tau}=-\frac{Ste^*}{\rho^*_{S-L}}\frac{1}{X}\frac{\partial\Theta}{\partial\xi}\left[1+\left(\frac{\partial X}{\partial\xi}\right)^2\right] \quad (20\text{-b})$$

5- Boundary conditions for the conductive wall-liquid interface

$$\Theta_W=\Theta_L \quad (21\text{-a})$$
$$k^*_{W-L}X\frac{\partial\Theta_W}{\partial\xi}=\frac{\partial\Theta_L}{\partial\xi} \quad (21\text{-b})$$

2.4 Heat Transfer Characteristics

2.4.1. The Average Nusselt Number at the Wall-Liquid PCM Interface

Equations (12-16) are solved with the relevant boundary conditions given by Eqs. (17-21) to determine the temperature, the vorticity and the stream function distributions. The local Nusselt number is calculated from the temperature distribution as:

$$Nu_y = \frac{-H_2}{\Delta T}\left(\frac{\partial T}{\partial x}\right)_{x=0} = -\left.\frac{\partial \Theta}{\partial \xi}\right|_{\xi=0}$$

The average Nusselt number at the wall-liquid phase interface is given by:

$$\overline{Nu}_{W-L} = \int_0^1 -\frac{\partial \Theta}{\partial \xi}\, d\eta \tag{22}$$

2.4.2. Average Nusselt Number for Melting Process

The average heat transfer coefficient based on the total energy input to the system Q_{tot} over the total elapsed time since the onset of the melting is defined by the following equation:

$$\bar{h} = \frac{Q_{tot}/t}{H_2 D\,(T_{W\text{-}L} - T_F)} \tag{23}$$

where;

$$Q_{tot} = \rho_W c_W (T_W - T_{W-L})\, V_w + \int_{V_S} \rho_S c_S (T_S - T_I)\, dV_S + \int_{V_L} \rho_L c_L (T_L - T_F)\, dV_L + \int_{V_L} \rho_L L\, dV_L \tag{24}$$

Where;

$T_W = (T_H + T_{W\text{-}L})/2$, $T_L = (T_{W\text{-}L} + T_F)/2$, $T_S = (T_F + T_I)/2$

So, the average Nusselt number can be given by:

$$\overline{Nu}_{tot} = \frac{\bar{h} H_2}{k_L} = \frac{Q_{tot}}{t D (T_{W-L} - T_F) k_L} \tag{25}$$

After substituting Q_{tot} in the above equation:

$$\overline{Nu}_{tot} = \frac{1}{\tau^* A_R}\left[\frac{\rho^*_{W-L} Sc_W}{2}\left(\frac{1}{\phi} - 1\right) + \frac{\rho^*_{S-L} Sc_S}{2} + \frac{V}{V_O}\left(1 + \frac{Ste^*}{2} - \frac{\rho^*_{S-L} Sc_S}{2}\right)\right] \tag{26}$$

where $\tau^* = \tau . Ste^*$, $Sc_w = c_W(T_H - T_{W\text{-}L})/L$ and $Sc_S = c_S(T_F - T_I)/L$

2.5 Finite Element Formulation

The immobilized transformed equations are formulated using the conventional Galerkin procedure [15-18], with the interpolation function as a weighted residual to derive the finite element equations. The finite element descritization in two-dimensional domain is carried out using linear triangular element. The temperature Θ^e, the vorticity Ω^e, and the stream function Ψ^e in the element can be represented in terms of the nodal values Θ_m , Ω_m , and Ψ_m respectively by a simple polynomial as follows:

$$\Theta^e = \sum_{m=1}^{3} N_m \Theta_m \;, \Omega^e = \sum_{m=1}^{3} N_m \Omega_m \;, \Psi^e = \sum_{m=1}^{3} N_m \Psi_m \tag{27}$$

Where;

N_m: is the usual interpolation function and defined by:

$$N_m = (1/2A)[a_m + b_m\xi + c_m\eta] \quad (28)$$

Where; A is the element area and;

$$a_1 = \xi_2\eta_3 - \xi_3\eta_2\ ,\ b_1 = \eta_2 - \eta_3\ , c_1 = \xi_3 - \xi_2 \quad (29)$$

The other components are given by cyclic permutation of the subscripts in the order 1, 2, and 3. If the approximations given by Eq. (27) are substituted in the governing Eqs. (12-16), and the global errors are minimized using the above interpolation functions N_i as weighting functions. After performing the weighted integration over the domain G and the application of Green's theorem, this present model can be written in the equivalent matrix form as:

$$[K_1]\{\Theta\} = \{F_1\}, \qquad [K_2]\{\Omega\} = \{F_2\}, \qquad [K_3]\{\Psi\} = \{F_3\} \quad (30)$$

where,

$$[K_1] = [K_I] + [K_{II}]$$

$$[K_I] = \sum_{e=1}^{E} \int_{G^e} \left(\frac{\partial [N]^T}{\partial \xi} \cdot \frac{\partial [N]}{\partial \xi} + \frac{\partial [N]^T}{\partial \eta} \cdot \frac{\partial [N]}{\partial \eta} \right) dG$$

$$[K_{II}] = \sum_{e=1}^{E} \int_{G^e} \left(\Psi_\xi \frac{\partial [N]}{\partial \eta} - \Psi_\eta \frac{\partial [N]}{\partial \xi} \right) dG$$

$$\{F_1\} = \sum_{e=1}^{E} \int_{\Gamma^e} \left([N]^T \frac{\partial T}{\partial \xi} + [N]^T \frac{\partial T}{\partial \eta} \right) d\Gamma$$

where;

E = total number of elements, G bounded domain,

Γ domain boundary,

$$\Psi_\xi = \frac{\partial \Psi}{\partial \xi}, \quad \Psi_\eta = \frac{\partial \Psi}{\partial \eta}$$

Similarly, $[K_2]$, $[K_3]$, $\{F_2\}$ and $\{F_3\}$ can be written in the same manner. Equations (30) give three sets of algebraic equations which have been solved by Gauss elimination method. The finite element formulation and the resulting linear equations were solved through a computer FORTRAN program.

3- MODEL VALIDATION

To check the consistency and reliability of the present analysis, the present model predictions are compared with experimental results and model predictions obtained from Bekermann and Viskanta [7] for ϕ=1.0 i.e. no wall. Gallium is used as a phase change material. The properties and experiments characteristics used for comparison are illustrated in Table (1).

Table (1): The properties and experiments characteristics [7]

Pr = 0.0208, α^*_{S-L} = 1.105, k^*_{S-L} =1.0, Sc_S =0.468,
ρ^*_{S-L} =0.969, Ra = 3.275x10^5, A_R =1.0, and ϕ =1.0

Figure (2a) shows the comparison between the measured experimental data [7], and the present model prediction for the temperature profile at different levels. Figure (2b) illustrates the comparison between the present model and the model used in [7] for determining the melting rate. From the figures, it can be concluded that the present model is in good agreement with the model used by Bekermann and Viskanta [7] as well as their experimental data.

4- RESULTS AND DISCUSSIONS

The effect of wall thickness, i.e., void fraction ϕ, which having the values of 0.98, 0.926, 0.862 and 0.757 respectively, for metallic and non-metallic materials at different Rayleigh and Stefan numbers on the molten volume fraction is illustrated in Fig. (3). From the figure, it is indicated that the void fraction has nearly no effect for metallic material (copper) which having a value of wall to liquid phase thermal diffusivity ratio of α^*_{W-L}=1350 and wall to liquid thermal conductivity ratio of k^*_{W-L}=2600 and this behavior takes place for all values of Rayleigh and Stefan numbers. But for non-metallic wall material (building brick) having a value of wall to liquid phase thermal diffusivity ratio of α^*_{W-L}=5 and wall to liquid thermal conductivity ratio of k^*_{W-L}=5, a considerable effect of void fraction on the on the melting rate is illustrated. Also, from the figure, it is shown that as the void fraction increases i.e. the wall thickness decreases, the rate of melting increases. This is due to the decreased thermal resistance of the wall. The average Nusselt number based on the total heat input to the system, which is given by the derived equation (26), represented as $Nu_{tot}/Ra^{*1/4}$, is illustrated in Fig. (4). This is for metallic wall material (a), and non-metallic wall material (b), for different Rayleigh and Stefan numbers. From the figure, it is shown that a sharp decrease of the average Nusselt at early times of melting process and this rapid decrease is larger for metallic wall than the non-metallic wall and this indicating that the conduction is the dominant mode of heat transfer. Then the average Nusselt number becomes nearly constant indicating that natural convection becomes the dominant mode of heat transfer. Also, it is shown from the figure that, the increase of the void fraction increases the Nusselt number for all times till reaching steady state condition.

Figure (5) shows a significant effect of void fraction on the timewise variation of the average Nusselt Number at the wall/liquid PCM interface at different Rayleigh and Stefan numbers for non-metallic wall material whereas the effect of void fraction for metallic wall is insignificant for all values of Rayleigh and Stefan number

Different expressions for the modified Rayleigh number are suggested and many numerical runs are made for these expressions. From the results of these numerical runs, It was concluded that: when the modified Rayleigh number is $(g\beta H_2^3(T_H - T_F)/\nu\alpha)$, the effect of wall properties disappeared. The effect of void fraction (wall thickness) disappeared when using modified Rayleigh number of $(g\beta H_2^3(T_H - T_F)/\nu\alpha)$. ($H_1/H_4$). So, in this investigation the modified Rayleigh number takes the expression $(g\beta H_2^3(T_{W-L} - T_F)/\nu\alpha)$ which represents the true Rayleigh number and gets the actual effects of wall thickness, wall properties, (design conditions) and Rayleigh and Stefan

numbers (operating conditions) on the melting rate and heat transfer characteristics for melting process in the enclosure. The effect of Rayleigh and Stefan numbers on the timewise variation of molten volume fraction, average Nusselt number based on the total heat input to the enclosure and the average Nusselt number at the wall-liquid phase interface for non-metallic wall is illustrated in Fig. (6). From the figure, it is noticed that as the Rayleigh and Stefan number increase the melting rate, the average Nusselt number at wall-liquid phase interface, and the average Nusselt number based on the total heat input increase. The same behavior is noticed for metallic wall is illustrated in Fig. (7).

The effect of wall properties represented by wall to liquid PCM thermal diffusivity ratio and wall to liquid PCM thermal conductivity ratio on the melting rate, average Nusselt number at the wall-liquid phase interface and the average Nusselt number based on the total heat input is illustrated in Fig. (8). From the figure, it is noticed that the effect of wall properties on the above variables is considerable for non-metallic materials but this effect is insignificant for metallic materials.

Figure (9a, b) shows the effect of wall properties on the timewise variation of modified Rayleigh and Stefan numbers respectively. From the figure, it is concluded that for metallic material both modified Stefan and Rayleigh numbers are almost constants and this is due to small temperature drop across the metallic wall and they are nearly equal to Rayleigh and Stefan numbers. Whereas both modified Rayleigh and Stefan numbers are sharply decreased at the start of melting process followed by an increase for sometime, finally they are decreasing as the melting process proceeds. This may results in decreasing the melting rate and this is clearly illustrated especially for small Rayleigh number and small void fraction.

The timewise motion of the melting front for $Ra=1.14x10^8$, $Ste=0.045$, and $\phi=0.757$ for metallic wall having $\alpha^*_{W-L}=1350$, $k^*_{W-L}=2600$, and non-metallic wall having $\alpha^*_{W-L}=5$, $k^*_{W-L}=5$ is illustrated in Fig. (10a, b) respectively. The front locations are having a constant time interval $\Delta\tau=0.018$ apart. At the start of melting process, the melting front interface motion is uniform across the height of the cavity (almost vertical). This behavior indicates that conduction is the dominant mode of heat transfer. As the time proceeds, the onset of natural convection is established in the top of the cavity and the front interface curvature increases. While at the bottom of the cavity, the front motion is very slowly and conduction is still the dominant mode of heat transfer. Also, as mentioned before from the figure, it is shown that the melting rate is decreasing as the time proceeds.

The transient stream function and isotherms contours for relatively low Rayleigh number, $Ra=10^4$, $Ste=0.137$, $\phi=0.926$ and high conductive wall material $\alpha^*_{W-L}=1350$, $k^*_{W-L}=2600$, at $\tau=0.053$, 0.265, and 0.593 are illustrated in Fig. (11). It is seen that the streamline contours are nearly vertical and parallel to the hot wall and the position of minimum stream function seemed to be at the mid plane of the melt layer indicating that the conduction is the dominant mode of heat transfer. It is noted that the flow in the melt regime has a single circulating zone. The flat distribution of stream function around the central core means that the flow is stagnant. The transient stream function and isotherms contours for relatively high Rayleigh number, $Ra=1.14x10^8$, $Ste=0.045$, $\phi=0.926$ and low conductive wall material $\alpha^*_{W-L}=5$, $k^*_{W-L}=5$ at $\tau=0.053$ and 0.108 is shown in Fig. (12). From the figure, it is shown that the intensification of the convection circulating flow is

indicated by the upward shifting of the vortex center to the region in the vicinity of the free surface. It was also found that the concentration of the streamlines in vertical direction which indicates that the velocity along the vertical wall and the melting front are higher than the velocities along the horizontal walls.

The results for the molten volume fraction and the average Nusselt number at the wall/liquid phase of PCM interface have been calculated over the ranges of Rayleigh number, void fraction, and thermal diffusivity ratios used. Correlation equations for the molten volume fraction and the average Nusselt number at wall-liquid phase interface have been obtained from the least squares fit of the numerical results as:

For metallic wall:

$$\frac{V}{V_o} = 0.78\,\tau^{0.522}\,Ra^{0.026} \tag{31}$$

for $\tau \le 0.6,\ 10^4 \le Ra \le 5.7x10^8$, with maximum deviation of ±7%

$$\overline{Nu}_w = 0.25\,\tau^{0.297}\,Ra^{0.203} \tag{32}$$

for $\tau \le 0.6,\ 10^4 \le Ra \le 5.7x10^8$, with maximum deviation of ±9%

For non-metallic wall:

$$\frac{V}{V_o} = 4.477x10^{-6}\,\tau^{0.7439}\,Ra^{0.672}\,\phi^{1.4247}\,\alpha^{*\,0.1794}_{W\text{-}L} \tag{33}$$

for $\tau \le 0.37, 1.14x10^8 \le Ra \le 5.7x10^8, 0.757 \le \phi \le 0.98, 5 \le \alpha^*_{W\text{-}L} \le 8$, with maximum deviation of ±10%

$$\overline{Nu}_w = 1.99x10^{-3}\,\tau^{0.5736}\,Ra^{0.4615}\,\phi^{3.67}\,\alpha^{*\,0.3738}_{W\text{-}L} \tag{34}$$

for $\tau \le 0.315, 1.14x10^8 \le Ra \le 5.7x10^8, 0.757 \le \phi \le 0.98, 5 \le \alpha^*_{W\text{-}L} \le 8$, with maximum deviation of ±12%

For metallic and non-metallic walls:

$$\frac{V}{V_o} = 0.464\,\tau^{0.54}\,Ra^{0.0366}\,\phi^{0.2511}\,\alpha^{*\,0.0647}_{W\text{-}L} \tag{35}$$

$$\overline{Nu}_w = 0.11147\,\tau^{0.369}\,Ra^{0.2215}\,\phi^{1.365}\,\alpha^{*\,0.1289}_{W\text{-}L} \tag{36}$$

for $\tau \le 0.6,\ 10^4 \le Ra \le 5.7x10^8, 0.757 \le \phi \le 0.98, 5 \le \alpha^*_{W\text{-}L} \le 1350$, with maximum deviation of ±14%

5- CONCLUSION

From the results reported in this paper, it may be concluded that:-

1- The front location, shape and the melting rate are predicted.
2- The heating conditions, (i.e. Stefan and Rayleigh numbers) have large effect on the melting rate and average Nusselt number at wall-liquid phase for both metallic and non-metallic walls
3- The void fraction has a large effect on the melting rate and the heat transfer characteristics for non-metallic wall and has insignificant effect for metallic wall.
4- The melting rate and heat transfer characteristics are affected to a large extent due to the variation of the wall-liquid phase thermal conductivity and diffusivity ratios

for non-metallic wall material whereas they are not affected greatly by the properties for metallic material.

5- At low Rayleigh numbers and high wall/liquid thermal conductivity and diffusivity ratios, where the conduction is the dominant mode for heat transfer large molten volume fraction can be obtained.

6- At small void fractions and small Rayleigh numbers for non-metallic wall material after some time, there is a decrease in the melting rate and this is due to the decrease in both modified Stefan and Rayleigh numbers.

7- There is a need for new definition of modified Rayleigh number and a new characteristic length other than the cavity height.

REFERENCES

1- Sparrow, E.M. Patinkar, S.V. and Ramadhyani, S. , "Analysis of Melting in the Presence of Natural Convection in the Melt Region", Journal of Heat Transfer 99, pp. 520-526, 1977.

2- C.J. Ho and R. Viskanta "Heat Transfer During Melting From Isothermal Vertical Wall", J. Heat Transfer 106, pp. 12-19, 1984.

3- D. Gobin, C. Benard and Gadgil, "Transient Phase Change in Two-Dimension Coupled with Convection in the Liquid Phase: Experiments and Numerical Simulation", Int. Conference On Numerical Methods for Transient and Coupled Problems; Venice, pp. 60-69, 1984.

4- M. Okada, "Analysis of Heat Transfer during Melting from a Vertical Wall", Int. J. Heat Transfer 27, pp. 2057-2066, 1984.

5- C. Benard, D. Gobin and A. Zaloni, "Moving Boundary Problem: Heat Conduction in the Solid Phase of a Phase Change Material during Melting Driven by Natural Convection in the Liquid", Int. J. of Heat Mass Transfer, Vol. 29, pp. 1669-1681, 1986.

6- Sakr, R.Y. "Melting Heat Transfer in Rectangular Enclosures - Experimental and Numerical Study", Ph. D. Thesis, Cairo University, Egypt, 1994.

7- Bekermann, C. and Viskanta, R., "Effect of Solid Subcooling on Natural Convection Melting of Pure Metals" J. of ASME, Vol. 111, pp. 416-424, 1989.

8- Rady, M. A., Satyamurty, V.V. and Mohanty, A. K., "Effect of Liquid Superheat during Solidification of Pure Metals in a Square Cavity" Heat and Mass Transfer, Vol. 32, 1997, pp. 499-509, Springer, Verlag, 1997.

9- Olson, D.A. and Glicksman, L.R., "Transient Natural Convection in Enclosures at High Rayleigh Number", ASME, J. of Heat Transfer, Vol. 113, pp. 635-642, 1991.

10-Kim, D.M. and Viskanta, R. "Effect of Wall Conduction on Natural Convection Heat Transfer is Square Cavity", J. of Heat Transfer, Vol. 107, pp. 139-149. 1984.

11-Du, Z. G. and Bilgen, E. "Coupling of Wall Conduction with Natural Convection in Rectangular Enclosure", Int. J. Heat Mass Transfer, Vol. 35, no. 8, pp. 1969-1976, 1992.

12-El-Shazly, K.M., "Effect of Conduction on Free Convection Across A Vertical Shallow and Square Cellular Structure", The 1ST International Conference for Advanced Trends in Engineering, MICATE'99, pp. 163-171, 1999.

13-Hawang, C. C., Senpulin, and Shen, L. "Effect of Wall Conduction and Interface Resistance on the Phase Change Problem", Int. J. Heat Mass Transfer, Vol. 37/13, pp. 1849-1855, 1994.

14-Oberkampf, W. I. "Domain Mapping for the Numerical Solution of the Partial Differential Equations", Int. J. of Numerical Methods in Engineering, pp. 211-223, 1976.

15-Rao, S. S., The Finite Element Methods in Engineering, Pergamon Press, 1982.

16-Baker, A.J., Finite Element Computational Fluid Mechanics, Hemisphere Publishing Corporation, New York, 1983.

17-Pepper, D.W. and Heinrich, J.C., The Finite Element Method, Hemisphere Publishing Corporation, New York, 1992.

NOMENCLAUTRE

SI units were applied for the whole dimensional variables used in this paper.

a_1,b_1,c_1	coefficients in Eq. (29)
A_R	aspect ratio
A	element area
c	specific heat
D	enclosure depth
E	total number of elements
{F}	vector array Eq. (30)
g	gravitational acceleration
G	computational domain
h.	heat transfer coefficient
H_1	enclosure length
H_2	enclosure height
H_3	wall thickness
k.	thermal conductivity
[K]	stiffness matrix Eq. (30)
$[K_c]$	heat capacity matrix
L	latent heat, J/kg
ΔN	dimensionless distance between two adjacent nodes in the normal direction to the wall
$N_{1,..,3}$	interpolation functions
P	pressure
Q_{tot}	heat input
{R}	unknown variable array, Eq. (30)
S	front location
T	temperature
t	time
u	velocity component in x-direction
U_o	reference velocity

Subscripts:-

F	fusion
H	hot
I	initial
l	lower
L	liquid phase of PCM
o	reference
S	solid phase of PCM
S-L	solid –liquid interface
u	upper
W-L	wall – liquid interface
W	wall

Superscripts:-

'	first derivative w.r.t η
″	second derivative w.r.t η
.	first derivative w.r.t. τ
e	element level
---	average value
T	transpose

Dimensionless Groups:-

τ	Dimensionless time =Froude number
τ^*	$= Ste^*.\ \tau$ = modified dimensionless time
k^*_{S-L}	solid-liquid thermal conductivity ratio
k^*_{W-L}	wall-liquid thermal conductivity ratio

U dimensionless velocity component in x-direction
v velocity component in y-direction
V dimensionless velocity component in y-direction
x, y Cartesian coordinate
X dimensionless front location

Greek letters

α thermal diffusivity
β coefficient of thermal expansion
$\Gamma_{1,2,3}$ domain boundary
ρ density
ϕ void fraction
= volume of PCM/enclosure volume
ψ stream function
Ψ dimensionless stream function
ω vorticity
Ω dimensionless vorticity
ξ,η dimensionless coordinates
Θ dimensionless temperature

Nu_y local Nusselt number at wall-liquid interface
$\overline{Nu}_{W\text{-}L}$ average Nusselt number at wall-liquid PCM interface
$\overline{Nu}_{tot}$ average Nusselt number based on the total input heat
Ra Rayleigh number
Ra^* modified Rayleigh number
Ste Stefan number
Ste^* modified Stefan number
Sc_w wall subcooling parameter
Sc_s solid subcooling parameter
α^*_{S-L} solid-liquid thermal diffusivity ratio
α^*_{W-L} wall-liquid thermal diffusivity ratio
ρ^*_{S-L} solid-liquid density ratio
ρ^*_{W-L} wall-liquid density ratio

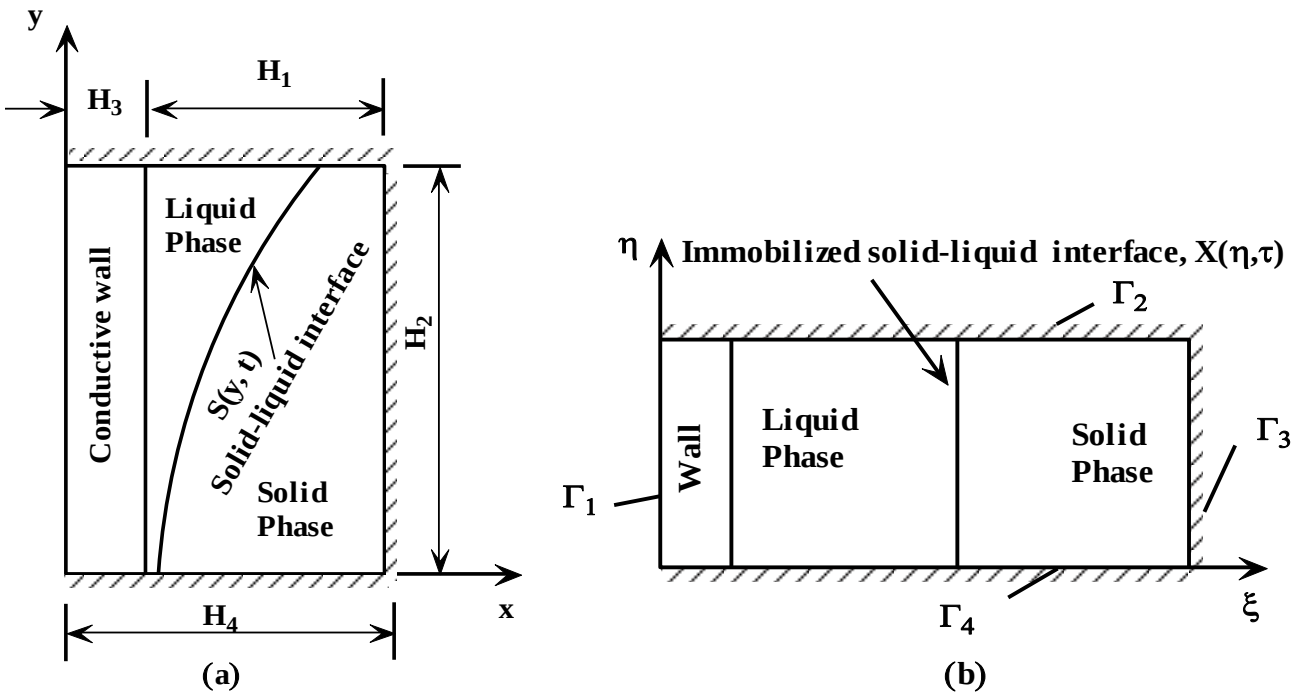

Fig. (1) Schematic diagram of the problem
(a): Conventional coordinate system (x, y, t)
(b): Immobilized coordinate system (ξ, η, τ)

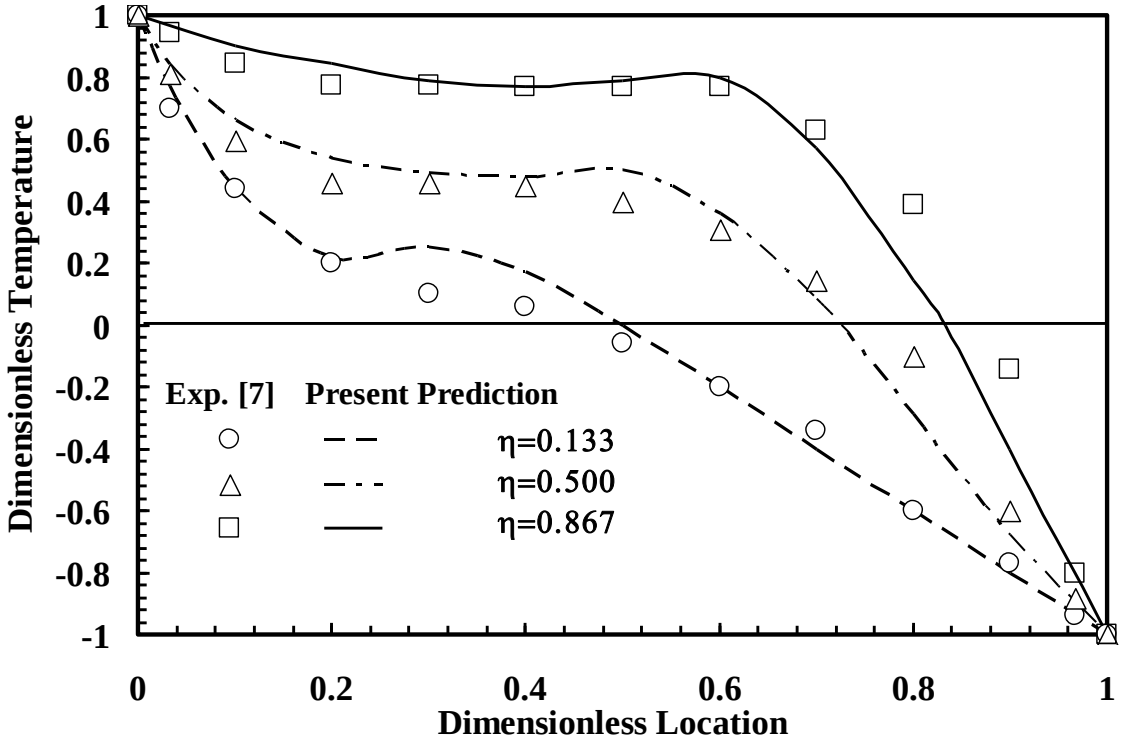

Fig. (2a) Comparison between the present predicted temperature distributions and experimental work [7]

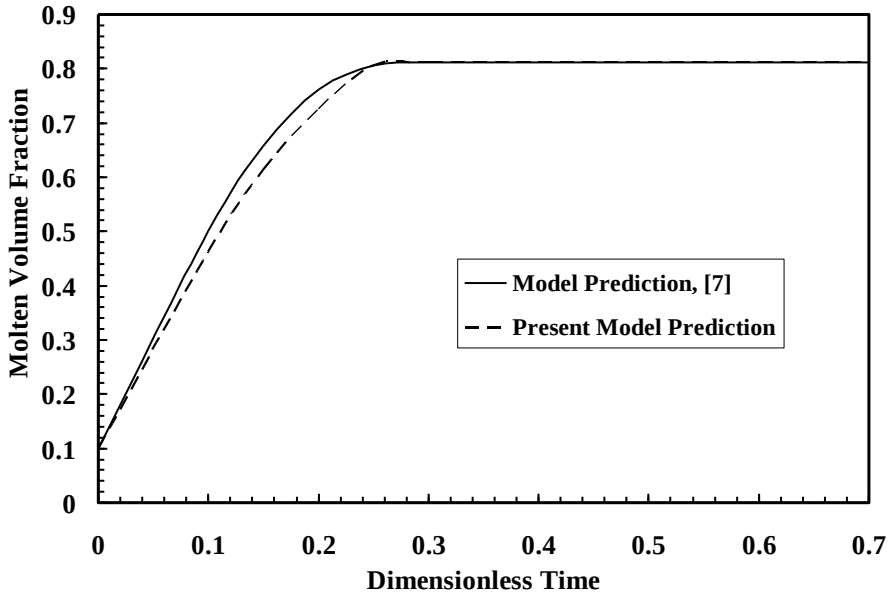

Fig. (2b) Comparison between the present model predictions for the melting rate and that predicted in Ref. [7]

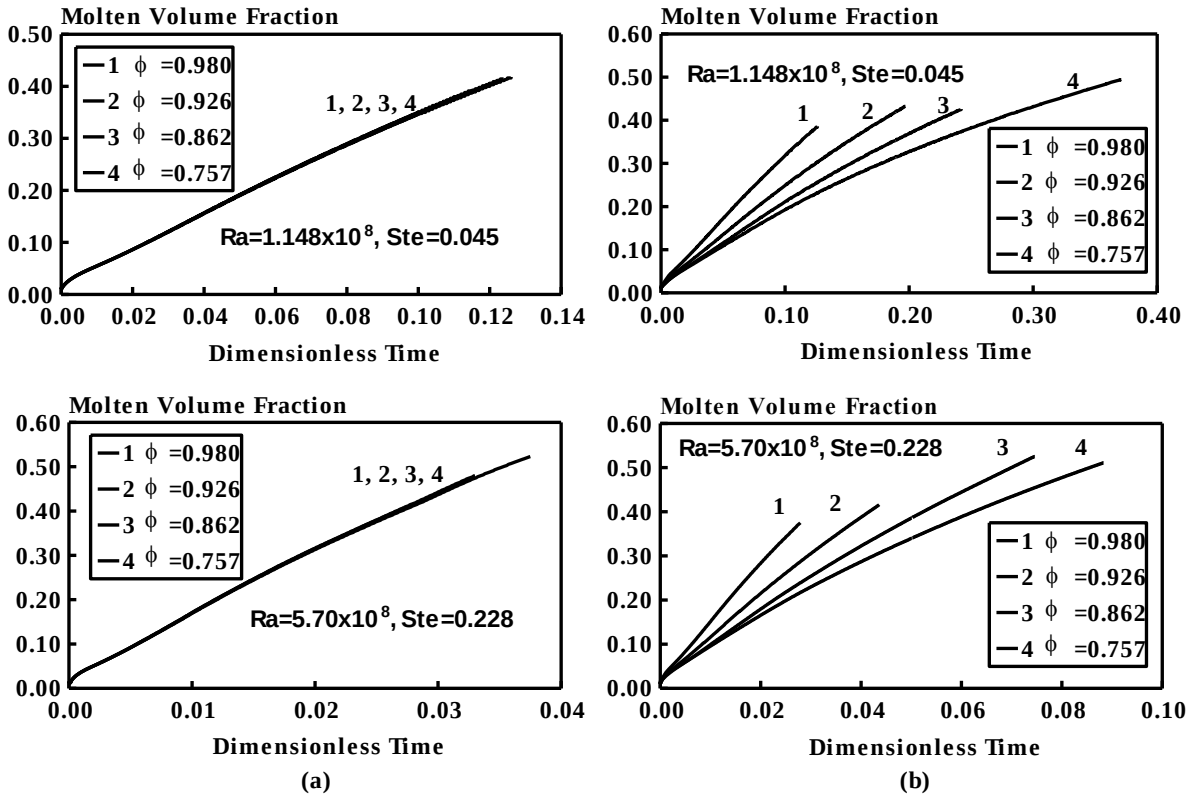

Fig. (3) Effect of void fraction on the melting rate at different Rayleigh and Stefan numbers for (a) metallic wall $k^*_{W-L} = 2600, \alpha^*_{W-L} = 1350$ **(b)** $k^*_{W-L} = 5, \alpha^*_{W-L} = 5$

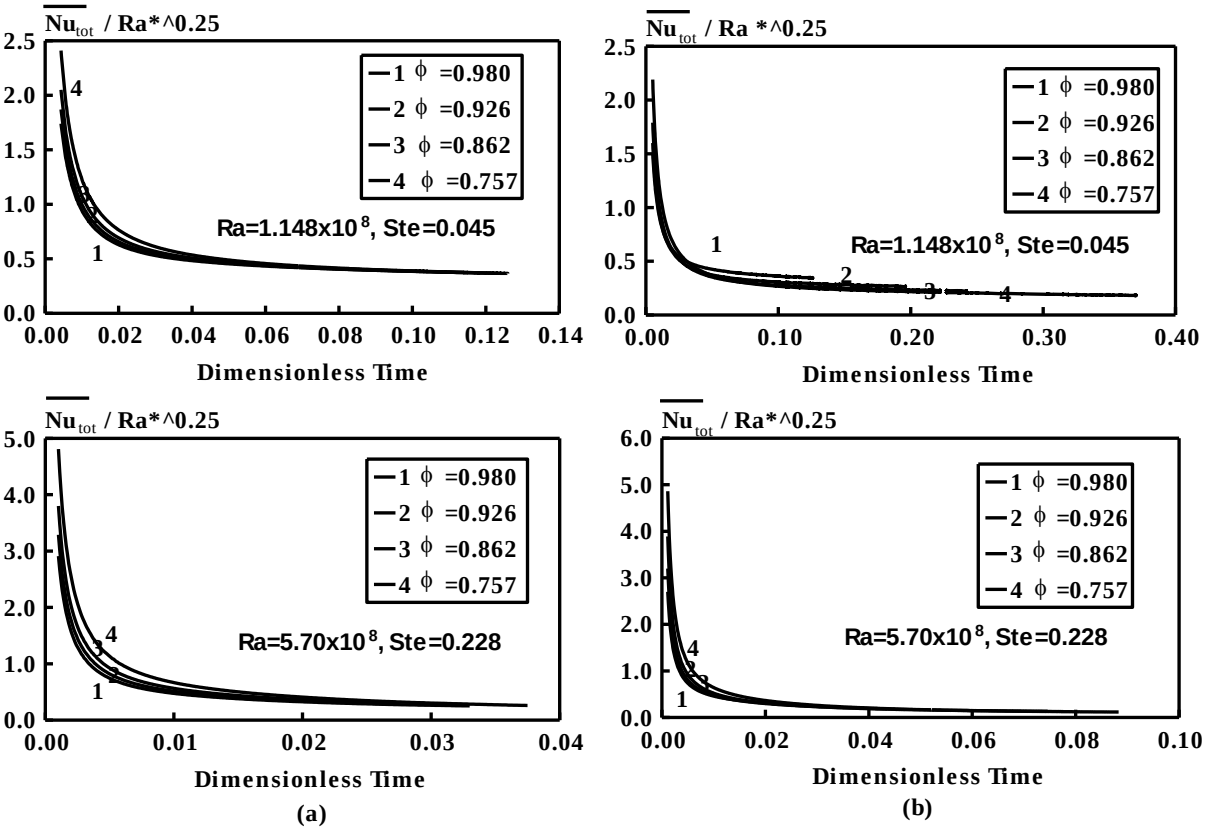

Fig. (4) Effect of void fraction on the average Nusselt number at different Rayleigh and Stefan numbers for (a) metallic wall $k^*_{W-L} = 2600, \alpha^*_{W-L} = 1350$ **(b)** $k^*_{W-L} = 5, \alpha^*_{W-L} = 5$

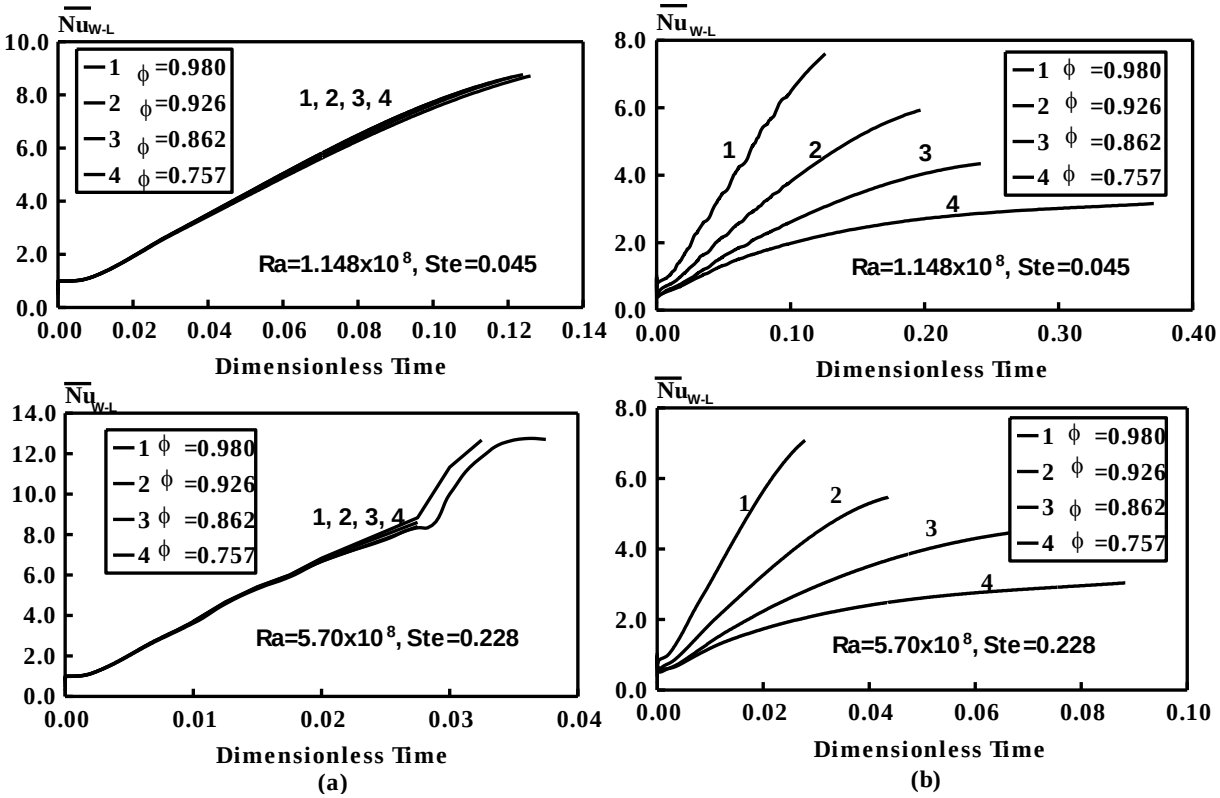

Fig. (5) Effect of void fraction on the timewise variation of the average Nusselt number at the wall-liquid PCM interface at different Rayleigh and Stefan numbers for (a) metallic wall $k^*_{W-L} = 2600, \alpha^*_{W-L} = 1350$ **(b)** $k^*_{W-L} = 5, \alpha^*_{W-L} = 5$

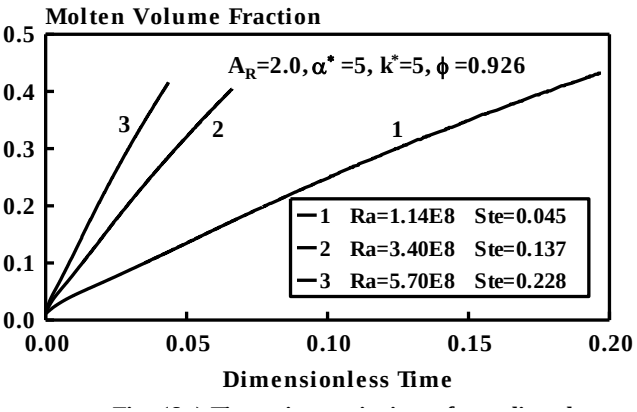

Fig. (6a) Timewise variation of predicted molten volume fraction for different Rayleigh and Stefan numbers

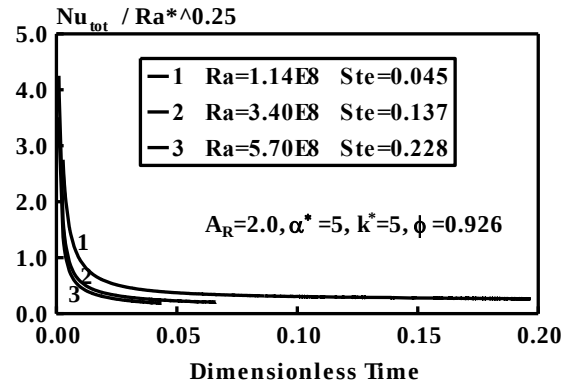

Fig. (6b) Timewise variation of the average Nusselt number for different Rayleigh and Stefan numbers

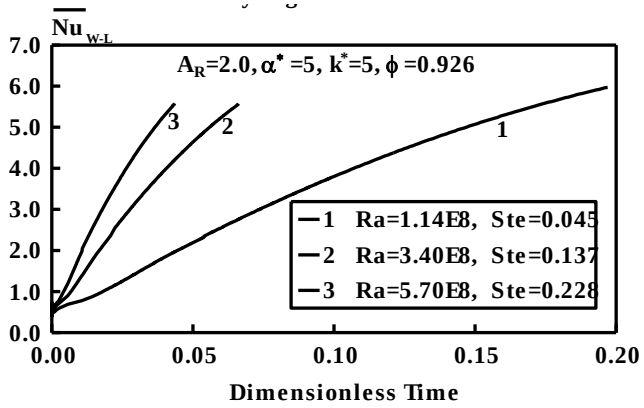

Fig. (6c) Timewise variation of the average Nusselt number at wall-liquid PCM interface for different Rayleigh and Stefan numbers

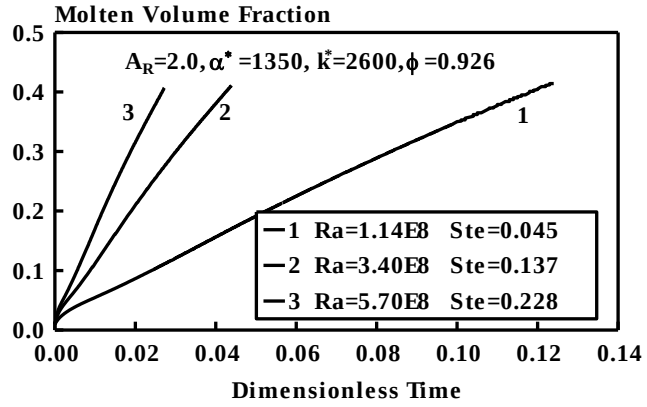

Fig. (7a) Timewise variation of predicted molten volume fraction for different Rayleigh and Stefan numbers

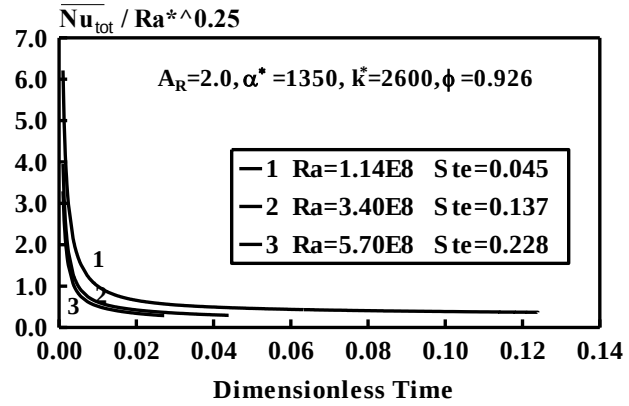

Fig. (7b) Timewise variation of the average Nusselt number for different Rayleigh and Stefan numbers

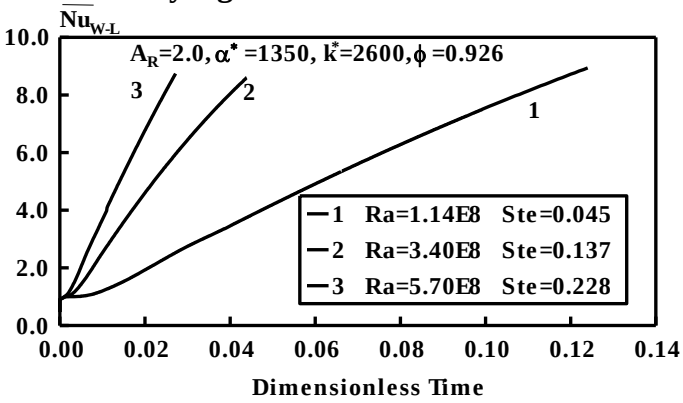

Fig. (7c) Timewise variation of the average Nusselt number at wall-liquid PCM interface for different Rayleigh and Stefan numbers

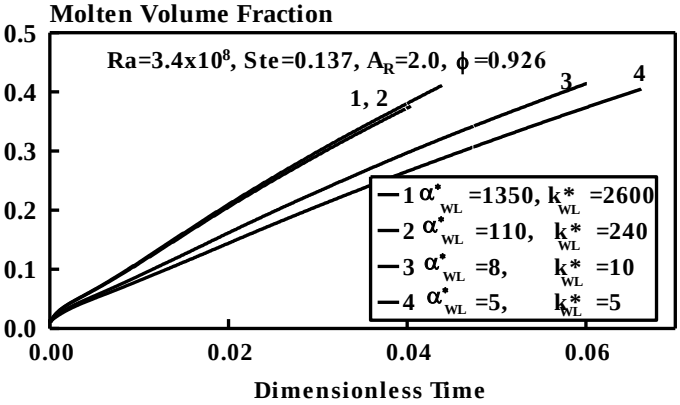

Fig. (8a) Timewise variation of predicted molten volume fraction for metallic walls 1, 2 and non-metallic walls 3, 4

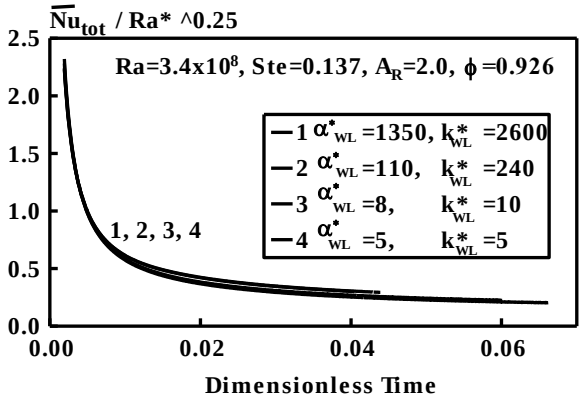

Fig. (8b) Timewise variation of the average Nusselt number for different Rayleigh and Stefan numbers

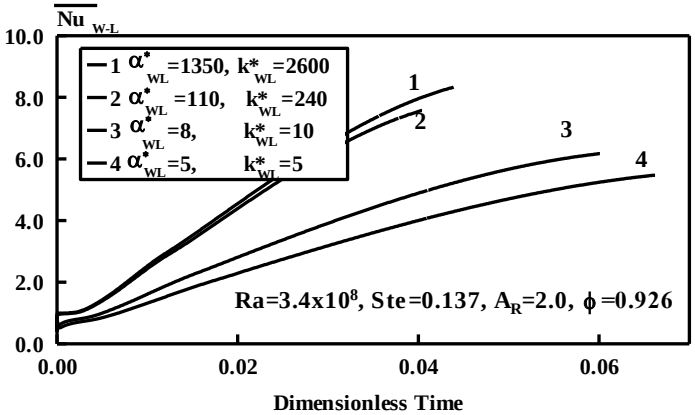

Fig. (8c) Timewise variation of the average Nusselt number at wall-liquid PCM interface for metallic walls 1, 2 and non-metallic walls 3, 4

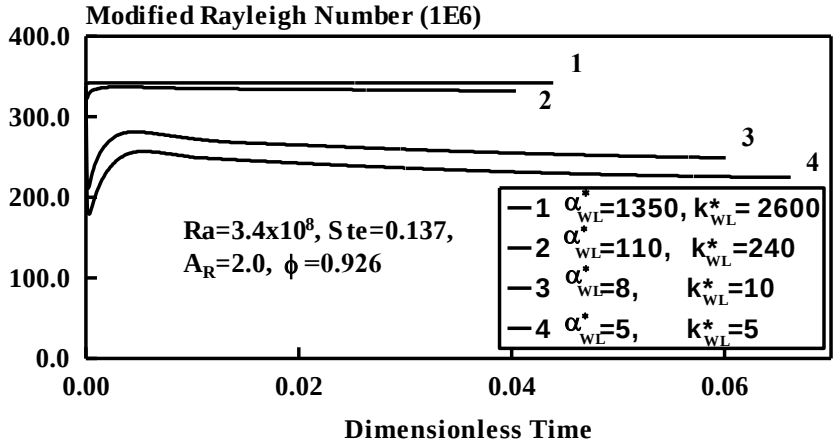

Fig. (9a) Timewise variation of the modified Rayleigh number for metallic walls (curves 1, 2), and non-metallic walls (curves 3, 4)

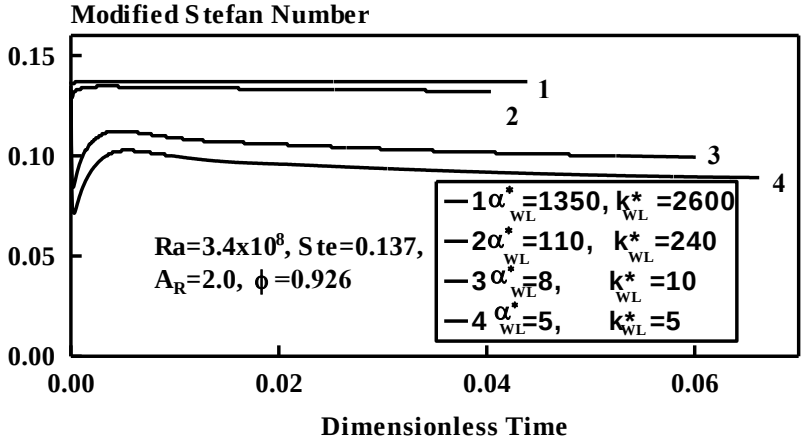

Fig. (9b) Timewise variation of the modified Stefan number for metallic walls (curves 1, 2) and non-metallic walls (curves 3, 4)

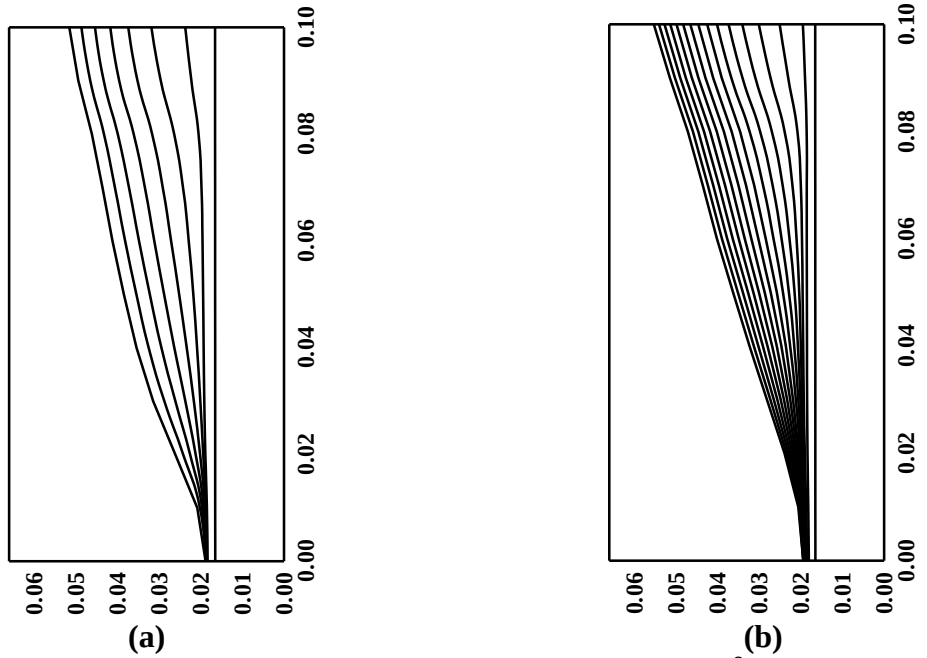

Fig. (10) Timewise motion of the melting front (Ra=1.14x10^8, Ste=0.045, ϕ=0.757, A_R=2 for (a) $k^*_{W-L}=2600, \alpha^*_{W-L}=1350$ (b) $k^*_{W-L}=5, \alpha^*_{W-L}=5$

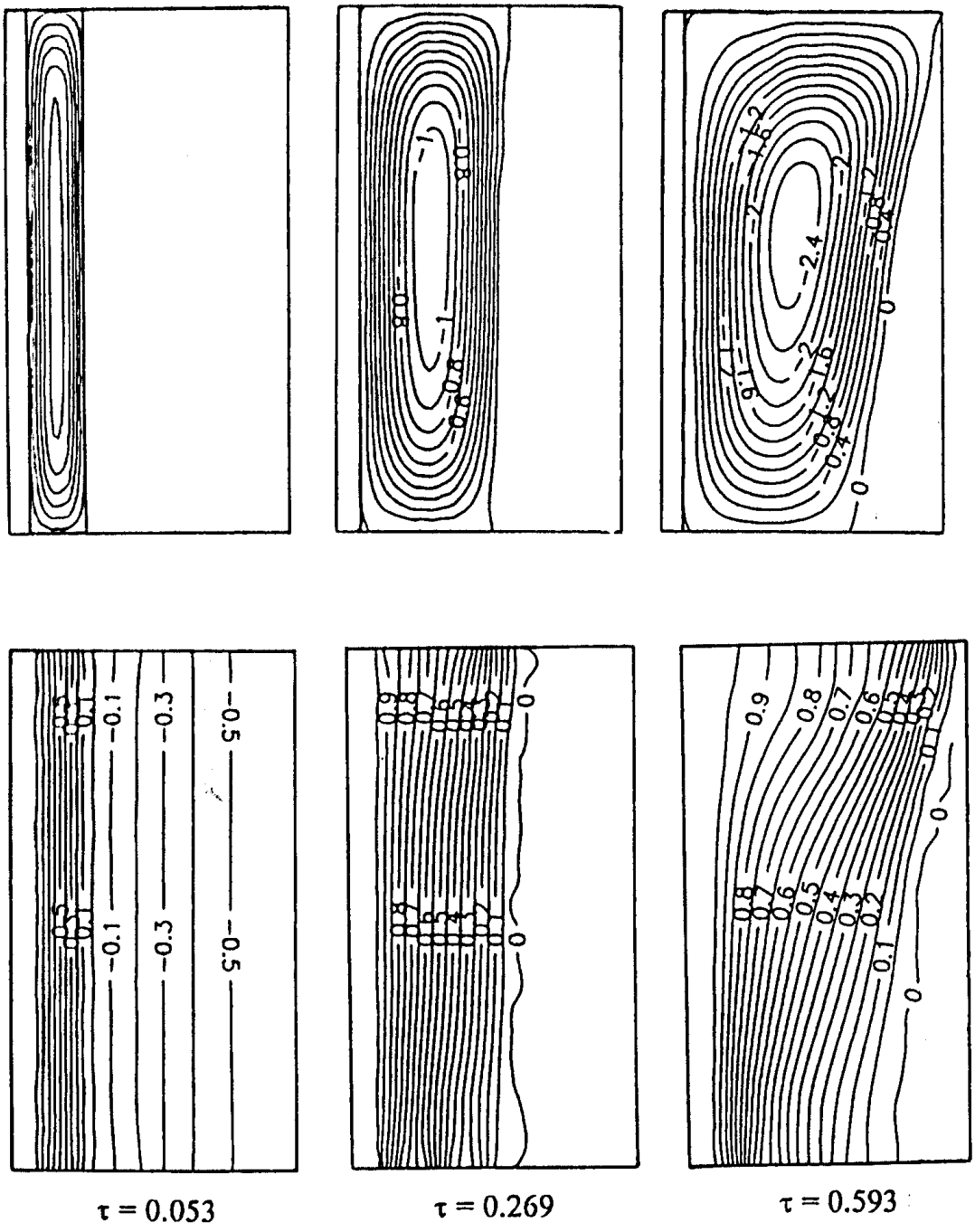

Fig. (11) Transient contours of stream function (top) and isotherms (bottom) (Ra=10^4, Ste=0.137, $k^*_{W-L} = 2600, \alpha^*_{W-L} = 1350, \mathrm{A_R} = 2.0, \phi = 0.926$**)**

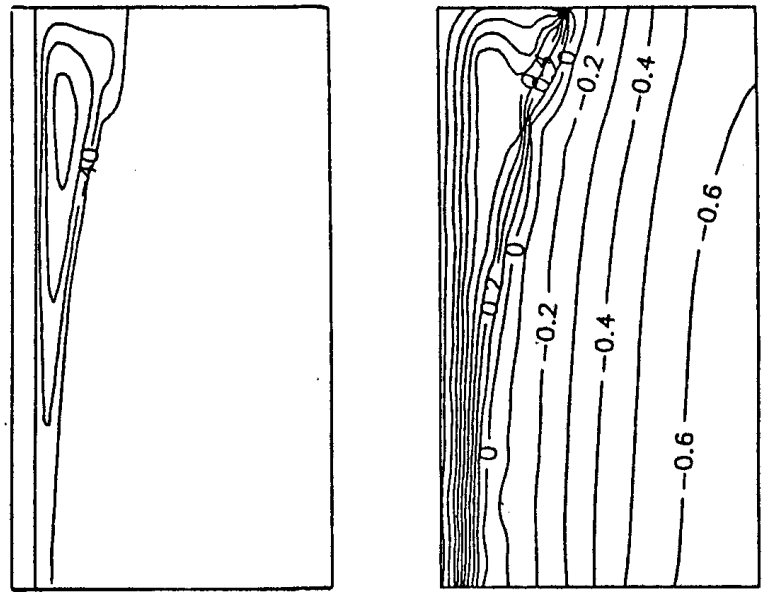

$\tau = 0.053$

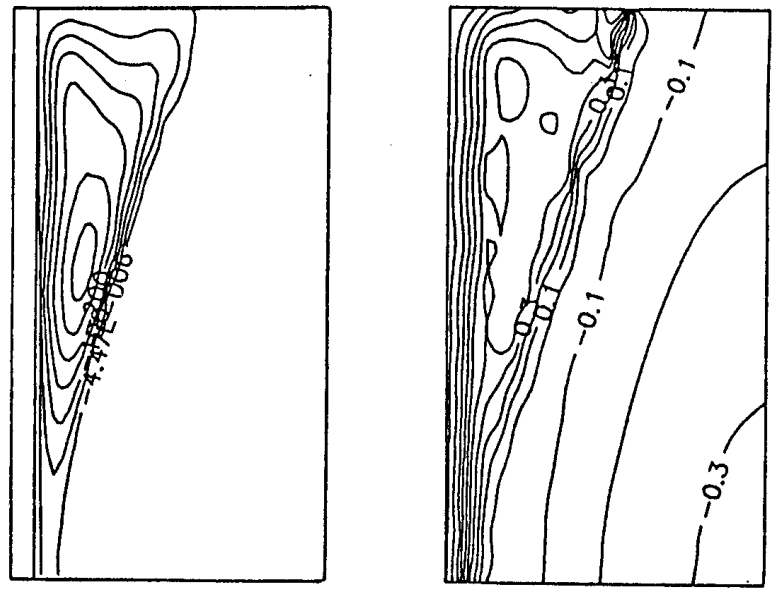

$\tau = 0.108$

Fig. (12) Transient contours of stream function (left) and isotherms (right) (Ra=10^4, Ste=0.137, $k^*_{W-L} = 2600, \alpha^*_{W-L} = 1350, \mathrm{A_R} = 2.0, \phi = 0.926$**)**